Draft version March 17, 2026
Typeset using LaTeX **twocolumn** style in AASTeX63

arXiv:2603.13736v1 [astro-ph.GA] 14 Mar 2026

Blackbody Quasar and Radio Source (BBQSORS): A Candidate of Transitional Little Red Dots with a $T \sim 10^4$ K Blackbody Spectrum

Yuxing Zhong [1], Xiaoyang Chen [2], Kohei Ichikawa [2,3], Youwen Kong [4], Kentaro Aoki [5], Satoshi Yamada [2,3,6], Tohru Nagao [7,8], Daisaburo Kido [9], Toshihiro Kawaguchi [10], Yoshiki Matsuoka [7], Toru Misawa [11], Shoichiro Mizukoshi [12], Masafusa Onoue [13], Ayumi Takahashi [14] and Yoshiki Toba [15,12,7]

[1] *Department of Physics, School of Advanced Science and Engineering, Faculty of Science and Engineering, Waseda University, 3-4-1, Okubo, Shinjuku, Tokyo 169-8555, Japan*
[2] *Frontier Research Institute for Interdisciplinary Sciences, Tohoku University, Sendai, Miyagi 980-8578, Japan*
[3] *Astronomical Institute, Tohoku University, Aramaki, Aoba-ku, Sendai, Miyagi 980-8578, Japan*
[4] *Institute of Astronomy, Graduate School of Science, The University of Tokyo, 2-21-1 Osawa, Mitaka, Tokyo, 181-0015 Japan*
[5] *Subaru Telescope, National Astronomical Observatory of Japan, 650 North A'ohoku Place, Hilo, HI 96720, U.S.A.*
[6] *Department of Astronomy, University of Geneva, Ch.d'Ecogia 16, 1290, Versoix, Switzerland.*
[7] *Research Center for Space and Cosmic Evolution, Ehime University, 2-5 Bunkyo-cho, Matsuyama, Ehime 790-8577, Japan*
[8] *Amanogawa Galaxy Astronomy Research Center, Kagoshima University, 1-21-35 Korimoto, Kagoshima 890-0065, Japan*
[9] *Research Center for the Early Universe, Graduate School of Science, The University of Tokyo, Bunkyo, Tokyo*
[10] *Graduate School of Science and Engineering, University of Toyama, Gofuku 3190, Toyama 930-8555, Japan*
[11] *Center for General Education, Shinshu University, 3-1-1 Asahi, Matsumoto, Nagano 390-8621, Japan;*
[12] *Academia Sinica Institute of Astronomy and Astrophysics, 11F of Astronomy-Mathematics Building, AS/NTU, No.1, Section 4, Roosevelt Road, Taipei 10617, Taiwan*
[13] *Waseda Institute for Advanced Study (WIAS), Waseda University, 1-21-1, Nishi-Waseda, Shinjuku, Tokyo 169-0051, Japan*
[14] *Faculty of Science, Kanagawa University, 3-27-1 Rokkakubashi, Kanagawa-ku, Yokohama, Kanagawa 221-8686*
[15] *Department of Physical Sciences, Ritsumeikan University, 1-1-1 Noji-higashi, Kusatsu, Shiga 525-8577, Japan*

(Received March 17, 2026)

Submitted to ApJL

ABSTRACT

JWST surveys have identified a new class of active galactic nuclei (AGN) called little red dots (LRDs). Their observational properties challenge the canonical AGN paradigm and provide key insights into the early growth phase of the supermassive black holes (SMBHs). We report Subaru/PFS spectroscopic follow-up of a radio-loud quasar at $z = 1.715$ from the UNVEIL radio AGN catalog and with X-ray detections. The spectrum displays broad C III]λ1909 and Mg IIλ2800 emission lines with FWHM $\gtrsim 3400$ km s^{-1}, accompanied by narrow absorption features. The spectrum reveals a characteristic Λ-shape over the rest-frame wavelength ranging $\sim$ 1500–3500 Å. The underlying continuum cannot be reproduced by simply applying dust extinction to typical unobscured quasars. Alternatively, it is well described by a blackbody spectrum with a temperature of $T \approx 10000$ K. This result agrees well with its UV to MIR photometry, which can be well modeled by three blackbody components representing the BH envelope ($T \approx 9700$ K), dust torus ($T \approx 1500$ K), and host galaxy dust ($T \sim 80$ K). The source is marginally detected in the GALEX NUV, revealing a potential V-shaped spectral energy distribution around 1400 Å, reminiscent of the spectral feature reported for LRDs whose V-shapes occur around 3000–4000 Å. This wavelength shift is broadly consistent with the temperature contrast between our blackbody component ($T \sim 10^4$ K) and the lower effective temperature of $T \sim 5000$ K expected for the BH envelope of LRDs. These properties suggest that this source might be caught in an evolutionary phase in which the dense gas envelope characteristic of LRD has begun to fragment, allowing us to witness the emergence of a quasar from an LRD-like state.

Corresponding author: Yuxing Zhong, Xiaoyang Chen, Kohei Ichikawa
yuxing.zhong.astro@gmail.com, xy.chen@astr.tohoku.ac.jp,
k.ichikawa@astr.tohoku.ac.jp

Keywords: galaxies: active — galaxies: nuclei — quasars: supermassive black holes

1. INTRODUCTION

One of the fundamental questions on supermassive black holes (SMBHs) is how they have grown up their masses from the first BH formation in the early Universe into the current values (e.g., Inayoshi et al. 2020). Recently, the James Webb Space Telescope (JWST) has opened a new window into high-redshift extragalactic astronomy, and one of its most important discoveries is a new population of active galactic nuclei (AGNs) known as little red dots (LRDs; Kocevski et al. 2023; Matthee et al. 2024). LRDs are ubiquitously found at $z > 4$ and they are characterized by the "V"-shaped rest-UV to optical spectral energy distribution (SED). They exhibit compact morphologies with red optical continua and broad Balmer emission lines (> 80%; Kocevski et al. 2025; Hviding et al. 2026), frequently accompanied by narrow absorption features (> 30%; Juodžbalis et al. 2024; Lin et al. 2024). However, most LRDs differ from typical type-1 AGNs in several respects, including the scarcity of UV/optical variability (Kokubo & Harikane 2025; Zhang et al. 2025a,b), the absence of strong X-ray emission (Ananna et al. 2024; Yue et al. 2024), and the weakness or even deficit of mid-infrared (MIR) emission from AGN-heated dust (e.g., Williams et al. 2024; Setton et al. 2025). Considering the overall energy budget, these findings suggest that the red optical SED is likely intrinsic rather than primarily driven by dust reddening (Li et al. 2025; Chen et al. 2025a).

A recent compilation of studies supports a scenario in which the central SMBHs of LRDs are enshrouded by Compton-thick dense gas with column densities of $N_{\rm H} \gg 10^{24}$ cm^{-2}. Such a configuration naturally gives rise to a "stellar-like" blackbody spectrum with temperatures of $T \sim$ 5000–7000 K. This temperature range readily accounts for the observed red rest-frame optical continua, while the optically thick gas can produce a Balmer break through absorption by collisionally excited hydrogen atoms populating the $n = 2$ level (Inayoshi & Maiolino 2025; Ji et al. 2025). Such an envelope may arise from a direct-collapse BH retaining a remnant envelope (Kido et al. 2025) or in a quasi-star environment for BHs forming through core collapse (Begelman & Dexter 2026). These gas-rich configurations can naturally suppress X-ray emission and potentially even radio emission, although super-Eddington accretion has also been proposed as a mechanism to account for the observed X-ray weakness (Inayoshi et al. 2025).

Another notable property of LRDs is their pronounced cosmic evolution in number density. Although LRDs are ubiquitously abundant at $z > 5$, reaching $\sim 10^{-4}$ Mpc^{-3} with a possible peak around $z \sim 7$ (Tanaka et al. 2025), recent JWST and wide-area ground-based surveys, such as Subaru/HSC, indicate a sharp decline in their number density at $z < 4$ (Ma et al. 2025a). Inayoshi (2025) proposed that LRDs represent a stochastic phase associated with the early growth of BHs, thus naturally reproducing the observed decline in their number density at $z < 4$. Interestingly, (Ma et al. 2025b) also predicted a sharp luminosity cutoff in the LRD luminosity function at $L_{\rm bol} \approx 10^{45}$ erg s^{-1}. Assuming Eddington-limited accretion, this luminosity corresponds to $M_{\rm BH} \lesssim 10^7\ M_\odot$, consistent with expectations from the gas-envelope model. This mass limit is also consistent with the maximum black hole mass expected from growth over a Salpeter timescale, which is comparable to the inferred LRD lifetime of $\sim 3 \times 10^7$ yr (Kido et al. 2025). This agreement suggests that the LRD phase may correspond to the initial episode of BH growth in the early Universe, particularly at $z > 4$.

In this framework, LRDs are characterized by gas-enshrouded accretion with a lifetime of $\sim 10^7$ yr. After a such enshrouded phase, the envelope should begin to disperse once the SMBH accretion rate exceeds the gas inflow rate from the host galaxy (Kido et al. 2025). In this stage, inflow from the interstellar medium (ISM) is hindered by radiation from the envelope, and the photospheric temperature rises to $\sim 10^4$ K (Hosokawa et al. 2012, 2013). This hotter-envelope phase may represent the final stage of the LRD episode, preceding the transition to an unobscured quasar. As the gas envelope disperses, the central engine becomes progressively exposed, allowing previously suppressed X-ray and possibly radio emission to emerge. Recently, two studies have reported LRDs, with detections of X-ray and/or radio emissions, in a possible transient phase, while both studies still have an expected envelope temperature of $T = 5000$–7000 K (Fu et al. 2025; Hviding et al. 2026).

In this Letter, we report a serendipitous discovery of Blackbody Quasar and Radio Source (hereafter BBQSORS), a radio and X-ray luminous AGN with merger feature at a spectroscopic redshift of $z_{\rm CIII} = 1.715$, which is based on the peak wavelength of CIII]λ1909 emission line. BBQSORS was originally selected as a radio bright quasar candidate by Very Large Array Sky Survey (VLASS) at 3 GHz (Lacy et al. 2020; Zhong et al. 2025). BBQSORS exhibits a blackbody-like UV-to-optical spectrum with $T \sim 10^4$ K, which is approximately a factor of two higher than the effective temperatures predicted for the SMBH envelopes proposed for LRDs. The spectrum is also associated with the broad Mg IIλ2800 emission with a narrow absorber reaching to the continuum level. BBQSORS also shows a V-shaped SED with a break wavelength around $\lambda \approx 1200$ Å, which is two times shorter than usual turning wavelength ($\lambda \approx$ 3000–4000 Å) of LRD-like V-shape. We discuss the origin

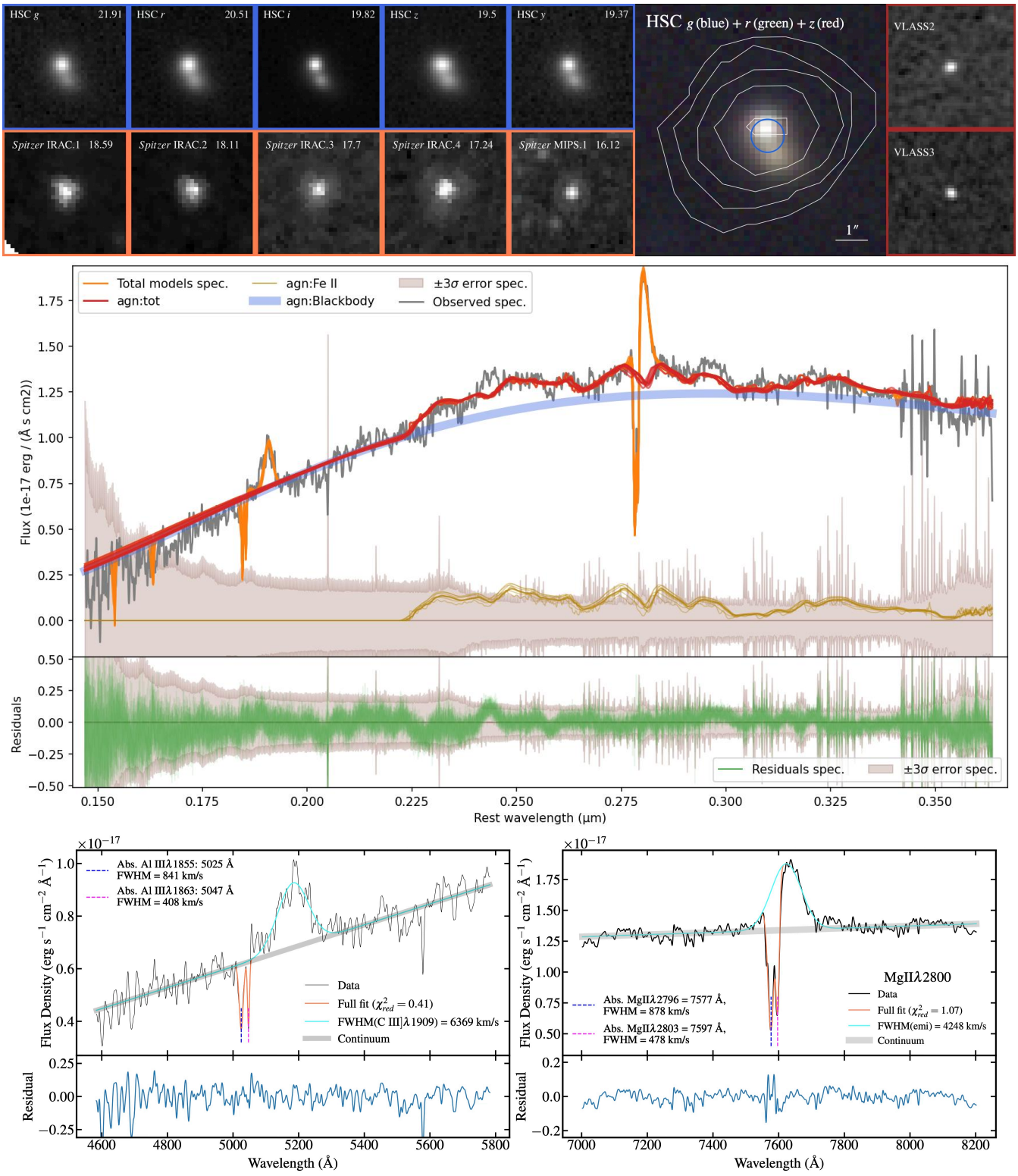

Figure 1. Overview of observations for the blackbody radio-loud quasar BBQSORS. *Top*: Optical images collected from Subaru HSC-SSP, IR images collected from *Spitzer*, and VLASS radio images at 3 GHz observed at Epoch 2 and 3. The false-color image is rendered using HSC $g + r + z$, overlaid with the white contours representing the VLASS Epoch 2 imaging. The blue circle represents the PFS fiber with a diameter of 1.″02. *Middle*: Subaru/PFS spectrum of BBQSORS and fitted using S^3`Fit`. *Bottom*: Zoom-in of the Subaru/PFS spectrum C III]λ1909 and Mg IIλ2800, as well as best-fits to the underlying continuum and emission/absorption, without incorporating the Fe II template. The spectra are Gaussian-smoothed by every 9 data points. For absorptions of Al III$\lambda\lambda$1855, 1863 and Mg II$\lambda\lambda$2796, 2803, we show their centers and FWHMs in the corresponding panels.

of the spectral features of BBQSORS and propose that BBQSORS might be in a transient phase of the LRD-like cocoon to an unobscured quasar. We adopt the following cosmological parameters throughout this paper: $H_0 = 68\,\mathrm{km\,s^{-1}\,Mpc^{-1}}$, $\Omega_M = 0.31$, and $\Omega_\Lambda = 0.69$ (Planck Collaboration et al. 2020).

2. MULTIWAVELENGTH PROPERTIES, SUBARU/PFS SPECTROSCOPY, AND RESULTS

2.1. *Morphology*

We show cutouts of BBQSORS in key wavelength bands in the top panel of Figure 1. Subaru/HSC cutouts (Aihara et al. 2018) reveal that there are two sources separated by $\sim 0\farcs7$ (corresponding to $\sim$ 6 kpc). The source in the top left represents BBQSORS and it coincides precisely with the centroid of 3 GHz radio emission observed by VLASS in Epochs 2 and 3. Because of the small separation between the two sources and the fact that the brightness of BBQSORS clearly dominates the system, the entire system has been treated as a single quasar, with a centroid offset from BBQSORS by approximately $0\farcs2$.

We performed aperture photometry on HSC cutouts for BBQSORS and its adjacent source by putting apertures on their centroids with a diameter of $0.5''$ and found that their photometry shows similar trends from g to z. As also supported by the similar colors in the HSC false-color image, this likely rules out the possibility that these two sources are located at very different redshifts. Therefore, throughout this letter, we treat BBQSORS as a radio quasar that resides in a galaxy merger.

2.2. *Subaru/PFS Spectroscopy and Spectral Fitting*

The Subaru/Ōnohi'ula Prime Focus Spectrograph (hereafter, PFS) UV-optical (Tamura et al. 2024) Spectroscopy for BBQSORS was obtained as a part of the community filler program (S25A0043QF PI: T. Nagao), which aims to re-observe already known quasars, of the Subaru/PFS Open Use program (Tanaka et al. in prep.). BBQSORS was included in the sample due to its classification as a quasar in Sloan Digital Sky Survey (Hall et al. 2002), and it was further identified to be radio-loud ($L_{3\mathrm{GHz}} > 10^{26}$ W Hz^{-1}) in the UNIONS-VLASS radio AGN catalog (Zhong et al. 2025; Gwyn et al. 2025). The centroid of the PFS fiber is based on the centroid of SDSS imaging and thus has an offset of $\sim 0\farcs2$ from BBQSORS and of $\sim 0\farcs6$ from the companion galaxy. Since PFS has a core fiber diameter of $1\farcs02$ (Tamura et al. 2024) and the typical seeing of PFS observations is < 1 arcsec, significant contamination of the nearby source is unlikely (see §2.4 for more information).

The PFS spectrum covers the observed wavelength of 3800 Å $< \lambda <$ 12600 Å with three separate spectrograph modules in the blue (3800–6500 Å), red (6300–9700 Å), and near-infrared (NIR; 9400-12600 Å) arms simultaneously with a spectral resolution of $R \sim 3000$. Data reduction was followed by a standard procedure of the PFS data reduction pipeline (M. Tanaka et al. in prep.). Currently, the PFS pipeline suffers from issues in flux calibration and sky subtraction in the red arm, resulting in negative flux values. We therefore restrict our analysis to wavelengths below 9900 Å.

The PFS spectrum (solid gray line) is shown in the middle panel of Figure 1 along with its best-fits using `S³Fit` (Chen 2025), and the fitting results are summarized in Table 1. This spectrum exhibits three distinct features. First, the spectrum shows broad emission lines in C III]λ1909 and Mg IIλ2800 with FWHM > 4000 km s^{-1} (bottom panel of Figure 1), without considering the strong Fe II emission around Mg IIλ2800. There also exist narrow absorbers associated with the MgII emission line with centers of 7576 Å and 7597 Å, respectively. The rest-frame separation between these two absorptions is about 7.4 Å considering $z = 1.715$, consistent with that of the Mg II$\lambda\lambda$2796, 2803 doublet. For Al III$\lambda\lambda$1855, 1863, the rest-frame separation is 8.1 Å. The Mg II$\lambda\lambda$2796, 2803 absorptions have velocity shifts of $v_{\mathrm{shift}} = -1886$ km s^{-1} and $v_{\mathrm{shift}} = -1060$ km s^{-1} with respect to Mg IIλ2800, respectively, in accordance with the outflow scenario. These results also suggest that the underlying continuum is unlikely to originate from the host galaxy stellar emissions.

The second feature is a clear Λ-shaped continuum, which is also present in the SDSS and DESI spectra of BBQSORS, indicating that it is robust and independent of the data reduction. This strongly curved spectrum is hard to reproduce the known blue spectral shape of unobscured quasars even if considering a de-reddening by an extremely high dust extinction (Richards et al. 2006; see §3.1 for further discussion). If the UV continuum is interpreted as that of a typical unobscured quasar, modeled with a single power law (PL) representing the accretion disk plus Balmer continuum, the best fit from `S³Fit` indicates that the continuum is dominated by the Balmer continuum, while the intrinsic accretion disk luminosity at 3000 Å is only $\sim 10^{32}$ erg s^{-1}. These results render such a model physically unrealistic. Alternatively, given that the Balmer continuum is often approximated in a blackbody form, the spectrum can be best described by a simple blackbody spectrum with a temperature of $T = 10002 \pm 550$ K with a low-level dust extinction of $A_V = 0.09 \pm 22$, as highlighted by the blue shaded region in the middle panel of Figure 1, which agrees well with the observed photometry (see §2.4).

Strong Fe II continuum emission (shown by the golden solid lines in the middle panel of Figure 1), particularly around $\sim$ 2800 Å and on the blue side of Mg IIλ2800, constitutes the third prominent spectral feature. Such a powerful Fe II emission may originate from collisional excitation attributed to low-ionization quasar outflows (Wang et al.

Table 1. Summary of the fitting results and physical properties

BBQSORS ($z_{\rm CIII}$ = 1.715[a]) RA = 214.79836, Dec = 52.09600[b]	
PFS	
$T_{\rm env,PFS}$	10002 ± 550 K
$L_{\rm env,PFS}$	$(3.7 \pm 1.2) \times 10^{45}$ erg s^{-1}
$A_{\rm V}$	0.09 ± 0.22
FWHM (BLR)	3356 ± 86 km s^{-1}
F(C III]λ1909)	$(15.3 \pm 0.8) \times 10^{-17}$ erg/s/cm^2
F(Mg IIλ2800)	$(51.6 \pm 3.3) \times 10^{-17}$ erg/s/cm^2
$T_{\rm env,ph}$	9742^{+282}_{-333} K
$L_{\rm env,ph}$	$(9.3 \pm 0.7) \times 10^{45}$ erg s^{-1}
$T_{\rm torus}$	1517^{+113}_{-112} K
$L_{\rm torus}$	$(5.7 \pm 0.2) \times 10^{45}$ erg s^{-1}
$T_{\rm dust}$	82^{+29}_{-16} K
$L_{\rm X}$	$2.7^{+1.4}_{-0.8} \times 10^{44}$ erg s^{-1}
$M^c_{\rm BH,MgII}$	$M_{\rm BH} = 2.5^{+6.3}_{-1.8} \times 10^8\ M_\odot$
$\lambda^c_{\rm Edd,MgII}$	$\lambda_{\rm Edd} \approx 0.28^{+1.00}_{-0.08}$

Notes. [a] z = 1.720 based on the broad Mg IIλ2800. [b] Centroid of BBQSORS. Centroids of PFS and the companion are RA = 214.798335, Dec = 52.095943, and RA = 214.79823, Dec = 52.09579, respectively. [c] We use FWHM(MgII) = 3356 km s^{-1} corrected for Fe II. $L_{\rm env,PFS}$ and de-reddened $L_{2100,\rm PFS}$ with $A_{\rm V}$ = 0.09 are adopted as conservative estimates.

2016), supported by the Mg II$\lambda\lambda$2796, 2803 absorption doublet. It is fitted adopting the Fe II template of the narrow line Seyfert-I galaxy, I Zw 1, which are combined from the works of Vestergaard & Wilkes (2001), Véron-Cetty et al. (2004), and Tsuzuki et al. (2006); these templates are all convolved to FWHM of 1100 km s^{-1}, i.e., the intrinsic FWHM of the employed combined template. Recently, thanks to higher resolution spectroscopy by JWST/NIRSpec, several LRDs (A2744-45924, Labbe et al. 2024; CAPERS-LRD-z9, Taylor et al. 2025) are now known to show Fe II lines in UV range (notably, 2000–3600Å; Labbe et al. 2024; Taylor et al. 2025), but optical Fe II lines are weak, mainly due to the low metallicity in the BLR (Kocevski et al. 2023; Trefoloni et al. 2025). This suggests that, at least for BBQSORS, it has abundant Fe II in the expected BLR, indicating that the metallicity is expected to be relatively higher than the currently known LRDs at $z > 3$.

2.3. *XMM-Newton X-ray Analysis*

The target was observed with XMM-Newton, which carries three European Photon Imaging Cameras (EPICs), on 2016 January 23 (ObsID 0765080801) and 27 (ObsID 0765080901) for exposures of 20 ks and 14 ks, respectively. We processed the data from the two EPIC/MOS cameras and the EPIC/pn camera using the XMM-Newton Science Analysis System (SAS; Gabriel et al. 2004) v21.0.0. The raw data were processed with the EMPROC and EPPROC scripts, and good events were selected with PATTERN ≤ 12 for MOS and PATTERN ≤ 4 for pn. Events during background flares were removed using thresholds of 0.15 counts s^{-1} in the >10 keV band for MOS and 0.3 counts s^{-1} in the 10–12 keV band for pn. Source spectra were extracted from a circular region with a radius of 20″, and background spectra from a nearby region with a radius of 40″. Ancillary response files and response matrix files were generated with ARFGEN and RMFGEN, respectively. However, only the pn data from January

Table 2. Summary of the photometries

Band	Flux[a] [μJy]	Error [μJy]	Ref.
GALEX NUV	0.428	0.043	1
CFHT/MegaCam u	1.361	0.147	2
CFHT/MegaCam r	23.828	0.116	2
SDSS g	4.835	0.481	3
SDSS r	20.324	0.880	3
SDSS i	41.153	1.365	3
SDSS z	57.863	5.329	3
PAN-STARRS g	7.688	0.805	4
PAN-STARRS r	18.885	0.704	4
PAN-STARRS i	37.225	0.246	2
PAN-STARRS z	41.679	1.839	4
PAN-STARRS y	52.048	3.054	4
HSC g	6.243	0.600	this work
HSC r	22.789	1.146	this work
HSC i	42.672	1.568	this work
HSC z	57.450	1.822	this work
HSC y	64.823	1.952	this work
WFCAM J	92.897	11.979	5
WFCAM H	90.365	18.310	5
WFCAM K	100.925	16.732	5
WISE 3.4 μm	155.946	1.905	6
WISE 4.6 μm	211.453	3.956	6
WISE 12 μm	436.418	84.813	6
Spitzer IRAC 3.6 μm	132.94	0.204	7
Spitzer IRAC 4.5 μm	207.16	0.335	7
Spitzer IRAC 5.8 μm	302.89	1.552	7
Spitzer IRAC 8.0 μm	462.83	2.927	7
Spitzer MIPS 24 μm	1.298×10^3	0.130×10^3	7
VLA 3 GHz	7.005×10^3	0.295×10^3	8
VLA 1.4 GHz	1.452×10^4	1.452×10^3	8

[a] The UV-to-IR photometric data are calculated for BBQSORS plus its adjacent source.
References: (1) Vanden Berk et al. (2020); (2) Gwyn et al. (2025); (3) Ahumada et al. (2020); (4) Magnier et al. (2020); (5) Schneider et al. (2025); (6) Cutri et al. (2021); (7) IRSA & SSC (2020); (8) Zhong et al. (2025).

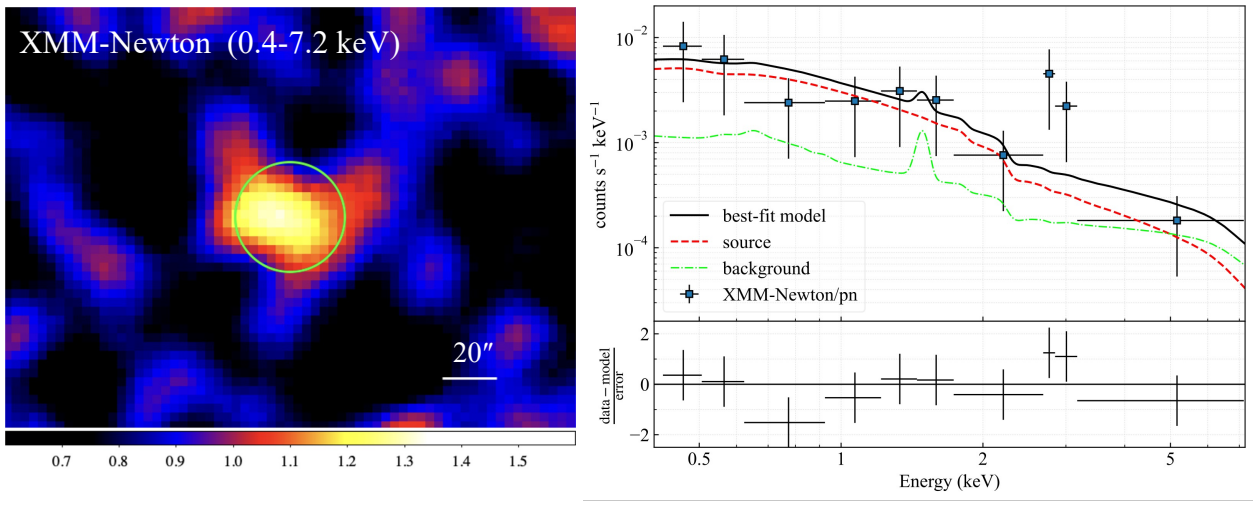

Figure 2. X-ray detection of BBQSORS with XMM-Newton. The left panel presents the EPIC/pn image in the 0.4–7.2 keV (rest-frame ∼1–20 keV) band, detected at a significance of 3.42σ. The green circle indicates the source region with a radius of 20″. The right panel shows the EPIC/pn spectrum folded with the energy response (blue squares) and the best-fitting model (black curve), consisting of source and background components. Residuals between the data and the model are shown in the bottom panel.

27 were usable, as the other observations were affected by high background flares and did not show significant source detection. In the left panel of Figure 2, we present a 0.4–7.2 keV (rest-frame ∼1–20 keV) pn image, where the source is detected at a significance of 3.42σ. The 4XMM catalog (DR9–13; Webb et al. 2020) reports a consistent ≈3σ detection in the 0.5–4.5 keV band, with no nearby X-ray sources within a 120″ region.

We simultaneously fitted the source and background spectra using the *C*-statistic. Galactic absorption was fixed at a hydrogen column density of $N_{\rm H} = 1.03 \times 10^{20}$ cm^{-2} (Willingale et al. 2013). The source emission was modeled as an absorbed PL (`zTBabs*zpo` in the XSPEC terminology) with the photon index fixed at $\Gamma = 1.8$. The background model included Galactic halo emission with a temperature of ∼0.25 keV and 0.2 solar metallicity, the cosmic X-ray background (absorbed PL with $\Gamma = 1.46$), the non–X-ray background (PL with $\Gamma = 0.24$), and an instrumental Ar Kα line at 1.487 keV (Leccardi & Molendi 2008; Cova et al. 2019). Owing to limited photon statistics, only the normalizations of the background components were allowed to vary.

The model adequately reproduces the spectra with ΔC/d.o.f. = 34.24/35 (see the right panel of Figure 2). The observed 0.5–7 keV flux is $F_{0.5-7\ \rm keV} = (2.16 \pm 0.69) \times 10^{-14}$ erg s^{-1} cm^{-2}. The best-fit parameters constrain the column density to $N_{\rm H} = 1.7^{+18.0}_{-1.7} \times 10^{21}$ cm^{-2} and the intrinsic 2–10 keV luminosity to $L_{\rm X} = 2.7^{+1.4}_{-0.8} \times 10^{44}$ erg s^{-1}. Adopting $\Gamma = 2.2$ yields a mildly higher obscuration, $N_{\rm H} \sim 1 \times 10^{22}$ cm^{-2}, while the luminosity remains nearly unchanged. These results indicate that BBQSORS hosts a luminous quasar with a very mild obscuration of $N_{\rm H} \sim 10^{21-22}$ cm^{-2}.

2.4. *UV to MIR Photometry*

Multiwavelength photometry has been compiled from UV to MIR (up to 24 μm), as well as from the radio (1.4 GHz and 3 GHz) and X-ray bands, which are summarized in Table 2. Because of the small separation (0.″7) between BBQSORS and its adjacent source, the recorded photometric data treat the two sources as an entity. Although HSC resolves the system into separate components, we performed forced photometry centered on the PFS fiber position using an aperture diameter of 2.″4 to enable a consistent comparison with the archived data, and the resulting measurements are listed in Table 2. Alternatively, placing the aperture on the centroid of BBQSORS results in fractional differences of as large as ∼ 6% across the *g* to *y* bands. We also performed a test by placing photometric apertures at the centroids of BBQSORS and the adjacent galaxy, respectively, adopting aperture radii ranging from 0.″05 to 0.″4, given their separation of ∼ 0.″7. The flux density ratio of BBQSORS to the galaxy reaches a maximum value of ∼ 3 at 0.″1 and remains above 2 up to 0.″4. Therefore, significant contamination from the adjacent galaxy is unlikely. Nevertheless, to conservatively account for any residual contribution from the neighboring source, we adopted a uniform 20% uncertainty on the observed flux densities in the SED fitting. We also incorporated a dust extinction curve in the PL form with $A_{\rm V} = 0.31$ based on the upper limit of the best-fit of the PFS spectrum.

Figure 3 shows the obtained UV to MIR SED and the best-fit. Similarly to the PFS spectrum that can be fitted with a single blackbody spectrum of $T_{\rm env,PFS} \approx 10000$ K, the rest-frame UV–optical photometry ranging 0.1–0.8 μm can also be described by a blackbody component of $T_{\rm env,ph} = 9742^{+282}_{-333}$ K

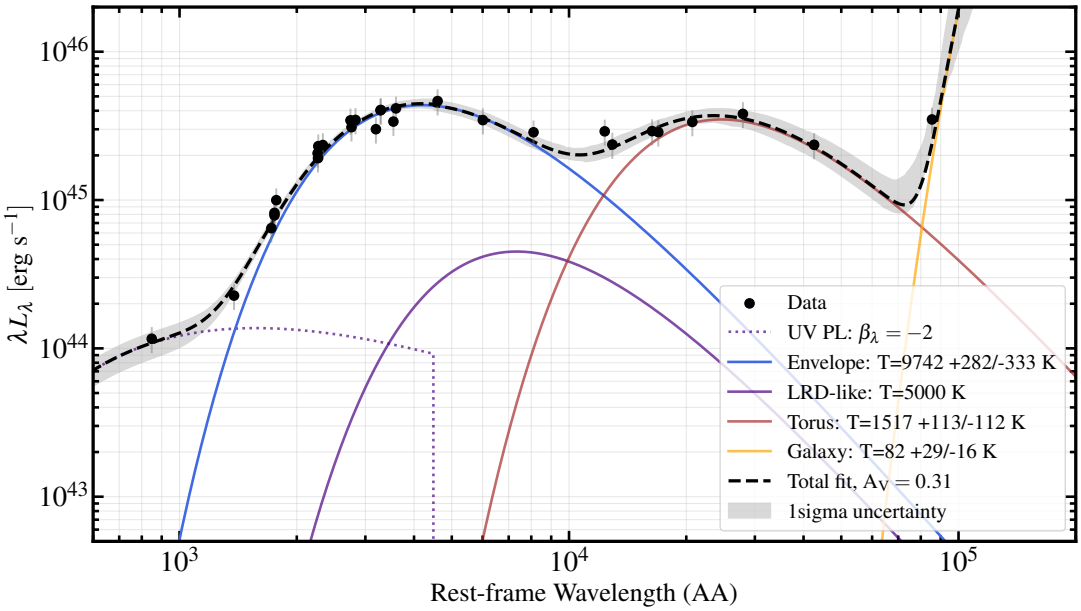

Figure 3. SED fitting for UV-to-MIR photometry with three blackbody components representing the SMBH envelope (blue), AGN dust torus (brown), and galactic dust (golden), plus a UV PL with fixed $\beta_\lambda - 2$, assuming $A_V = 0.31$ derived from the PFS spectrum. The purple solid line represents an LRD-like MBB component with $T = 5000$ K and $\beta_{MBB} = 0$, with its amplitude scaled according to $L \propto T^4$. The dust-extincted UV PL continuum intersects with the blackbody component originating from the accretion disk/LRD envelope, reproducing the LRD-like V-shape.

representing an optically thick gaseous structure surrounding the SMBH, i.e, the SMBH envelope. The IR continuum up to about 5 μm can be naturally reproduced by involving an AGN dust torus of $T_{torus} \approx 1500$ K. The increase in the flux density at $\lambda_{obs} = 24$ μm can be explained by introducing the galactic dust. Lacking IR observation at longer wavelengths, the galactic dust temperature is left poorly constrained to be $T_{dust} \approx 80$ K.

The SED of BBQSORS has an excess at $\lambda_{rest} \approx 850$ Å. This flux density is marginally above the detection limit of GALEX NUV (25.1 AB mag; Vanden Berk et al. 2020). This excess cannot be explained by a single blackbody component in the UV regime. We then assumed a UV continuum in the PL form adopting a spectral slope of $\beta_\lambda = -2$ (defined as $F_\lambda \propto \lambda^{\beta_\lambda}$) that is commonly observed for LRDs (Kocevski et al. 2023), which is consistent with the non-detection in the GALEX FUV band (24.0 AB mag; Vanden Berk et al. 2020). This UV PL component is incorporated into the SED fitting with $A_V = 0.31$. The resulting dust-extincted UV PL intersects with a blackbody component of $T_{env,PFS} \approx 9700$ K, produces an LRD-like V-shaped feature around $\lambda_{obs} \approx 1400$ Å. The optical-to-IR continua of LRDs are often modeled using the modified blackbody (MBB) model that depends on a PL slope β_{MBB} (de Graaff et al. 2025). Assuming an LRD-like blackbody component with $T = 5000$ K and $\beta_{MBB} = 0$ (de Graaff et al. 2025), with the amplitude scaled according to $L \propto T^4$, we find that this model reproduces the characteristic LRD V-shaped feature at a rest-frame wavelength of $\lambda_{rest} \approx 3400$ Å (purple solid and dotted lines in Figure 3). Given the marginal detection of NUV and the potential contamination from the companion galaxy, the robustness and origin of this UV excess remain unclear, and future observations are required to constrain the emission origins.

3. DISCUSSION

3.1. *Is BBQSORS red quasar or a different population?*

Based on the large spectroscopic survey of SDSS, a subset of quasars was identified because of their extreme red color in the UV continuum, which exhibits a clear curvature and cannot be well explained by a PL continuum (Richards et al. 2003). This population is commonly referred to as red quasars (hereafter rQSOs), the majority of which are reddened by intervening dust (Richards et al. 2003; Hopkins et al. 2004; Klindt et al. 2019). The levels of dust extinction range from up to $A_V = 0.7$ for those at $z \sim 1.5$ (Fawcett et al. 2022) to $E(B-V) = 1.5$ for the extremely dust-reddened populations (Urrutia et al. 2009). Additionally, rQSOs have a high incidence in moderate radio luminosity of $L_{1.4GHz} \sim 10^{25-27}$ W Hz^{-1} (Klindt et al. 2019; Rosario et al. 2021).

BBQSORS has a 1.4 GHz spectral luminosity of $L_{1.4GHz} \sim 2 \times 10^{26}$ W Hz^{-1}. It exhibits an exceptionally steep UV spectral slope across 1000–2000 Å in both spectroscopic and photometric data ($g - i > 2$). This is clearly demonstrated by the comparison between BBQSORS and the median spectrum of normal quasars shown in Figures 4 and 6. These properties

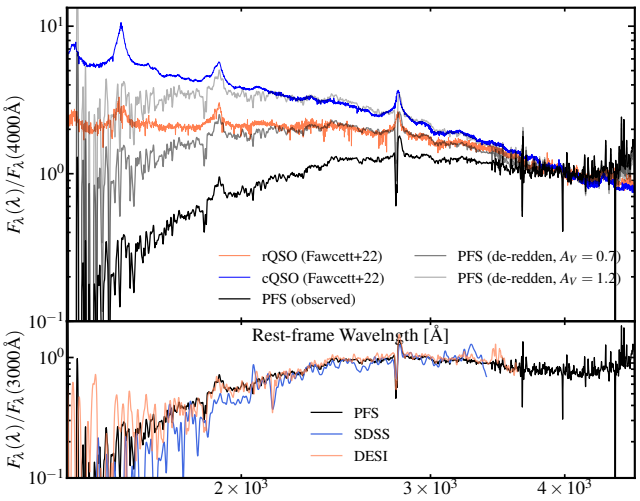

Figure 4. *Upper*: Comparison of the spectrum for BBQSORS with the median spectra of typical blue quasars (cQSOs) and of red quasars (rQSOs) suffering moderate dust reddening (Fawcett et al. 2022), where all spectra are normalized at 4000 Å. We de-redden the PFS spectrum assuming a PL dust extinction curve with A_V = 0.7 and A_V = 1.2. Although the de-reddened PFS spectrum have similar spectral shapes with cQSOs and rQSOs from about 2200 Å to 4000 Å, there are large discrepancies at the blue end. *Lower*: Comparison of PFS, SDSS, and DESI spectra for BBQSORS, where all are normalized at 3000 Å.

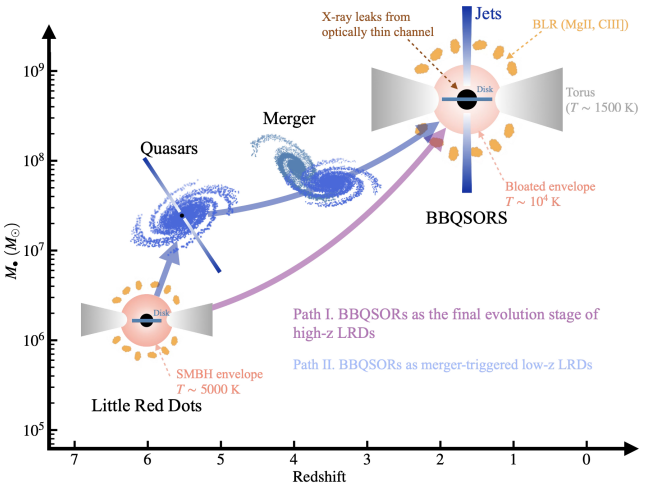

Figure 5. The evolution path of high-z LRDs to low-z BBQSORS.

are in line with the characteristics of rQSOs. We therefore compare the PFS, SDSS, and DESI spectra of BBQSORS with the median spectra of typical blue quasars (cQSOs) and of red quasars (rQSOs) that are moderately dust-reddened (Fawcett et al. 2022) by normalizing all spectra to 4000 Å. We de-redden the PFS spectrum assuming a dust-extinction curve in the PL form. At ∼ 2200–4000 Å, the de-reddened PFS spectrum agrees well with rQSOs assuming A_V = 0.7 and shows good consistency with cQSOs assuming A_V = 1.2. However, at shorter wavelengths ($\lambda_{rest} \lesssim 2000$ Å), there exist large discrepancies between the de-reddened PFS spectra and cQSOs and rQSOs. Adopting an SMC-like dust extinction curve instead yields the same result and even requires A_V = 2.7. These large discrepancies come from the highly curved spectral feature of BBQSORS, which is robust for its existence in PFS, SDSS, and DESI. If normalizing the spectra at 3000 Å, larger A_V is required for all extinction curves while the discrepancies at the blue end remain. In conclusion, the blackbody quasar BBQSORS mimics rQSOs rather than being the exact same population, although it may represent the progenitors of rQSOs, depending on the evolution of the structures surrounding the SMBH.

3.2. *BBQSORS as a transitioning LRD candidate*

3.2.1. *What does $T \approx 10^4$ K indicate in the context of LRDs?*

Recent theoretical studies suggest that the red color in the optical of LRDs can be maintained by a massive, optically thick gaseous envelope that surrounds the central accreting black hole and reprocesses the intrinsic emission into a cool optical–NIR SED (Inayoshi & Ho 2025). In particular, Kido et al. (2025) demonstrated that such an envelope can gravitationally confine radiation-driven outflows launched by super-Eddington accretion, allowing the system to radiate near the Eddington limit while sustaining an extended effective photosphere with temperatures close to the Hayashi limit, $T_{eff} \sim (5–7) \times 10^3$ K. In this regime, the envelope efficiently absorbs and re-emits the central radiation, suppressing strong feedback, and enabling gas to continuously infall from the surrounding ISM.

As the central black hole grows, however, the accretion rate required to sustain near-Eddington luminosities increases in proportion to the black hole mass, whereas the ISM inflow rate feeding the envelope may remain approximately constant. Once the mass supply becomes insufficient to replenish the envelope losses, the envelope mass gradually declines and the structure becomes patchy, leading to a covering factor below unity (Hviding et al. 2026). The X-ray source may therefore become visible through optically thin channels, while radio jets may drill through the envelope and further enhance the detectability of the X-ray emission. Kido et al. (2025) further showed that a photosphere can emerge either within the SMBH envelope or in the infalling material. When the effective photospheric temperature approaches $T \sim 10^4$ K, corresponding to the onset of hydrogen ionization, the envelope structure becomes unstable due to the rapid increase in thermal pressure and enhanced radiation–matter coupling. At this stage, gravitational confinement weakens, allowing radiation-pressure–driven outflows to escape and ultimately leading to rapid dispersal of the envelope.

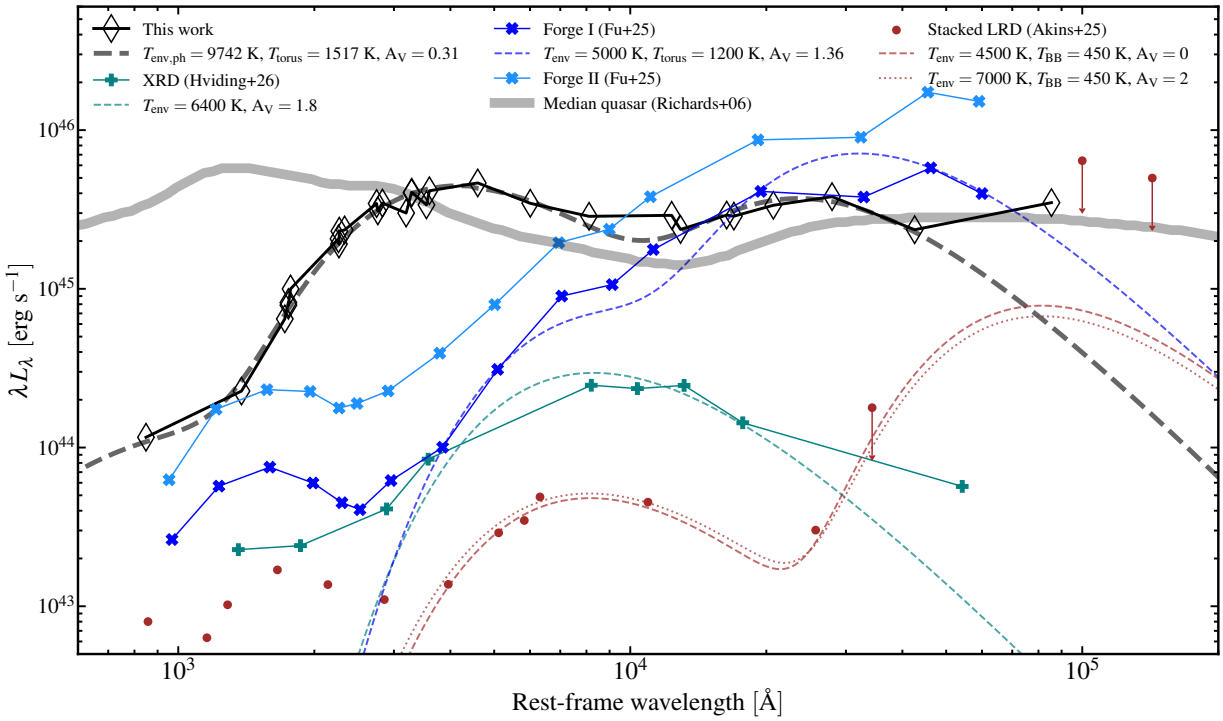

Figure 6. Photometry comparisons between the blackbody quasar BBQSORS, X-Ray Dot (Hviding et al. 2026), transitioning LRDs (Forge I and II; Fu et al. 2025), and stacked LRDs at $z \sim 6$ (Akins et al. 2025), which are indicated by solid lines with markers. The optical and IR continua of these sources can be in general fitted by blackbody models of different temperatures and suffering various dust extinction, which are indicated by dashed and dotted lines. We also supplement the median spectrum of normal quasars (Richards et al. 2006) for comparison.

This transition near $T \sim 10^4$ K therefore marks a critical evolutionary phase, in which the system shifts from an envelope-dominated, reprocessed state to a feedback-dominated phase characterized by strong mass loss and partial exposure of the central engine. In this picture, LRDs with cool blackbody-like SEDs trace an early, bloated-envelope phase, while sources exhibiting higher effective temperatures and emerging X-ray or radio emission represent a short-lived blown-out phase preceding the emergence of an unobscured quasar.

We speculate on the evolution path of the blackbody quasar BBQSORS in Figure 5. In the first scenario, the central SMBHs of LRDs continuously gain their masses, and once the SMBH exceeds a certain threshold such that the SMBH envelope can no longer sustain a steady state, we are witnessing the final evolution stage of LRDs. In the second scenario, LRDs have already evolved beyond the envelope-enshrouded phase, becoming high-z quasars or AGNs. Their SMBHs remain at relatively low accretion rates. Then, at a certain time, they encounter a nearby galaxy and start galaxy merging/interactions. The intense gas inflow accompanied by these events leads to a massive accretion onto the SMBH. If the inflowing material is beyond the capability of the SMBH to consume, as a result, an optically thick gas envelope forms, pushing the system into an LRD-like state. This second scenario may also provide an explanation for the LRD-like source at $z \approx 0.4$ that also resides in a merger (Chen et al. 2025b). These descriptions remain qualitative, as quantitative analysis is uncertain due to the limitations of the current observations. Follow-up observations of BBQSORS, as well as studies of larger samples, will be required to test these scenarios.

3.2.2. *Comparison with transition-LRD candidates*

A few objects have been argued to be LRDs in transitions, including the X-ray Dot (Hviding et al. 2026, XRD;) at $z = 3.28$ and two unusual LRDs at $z \approx 2.9$ (Fu et al. 2025, hereafter Forge I and II). We here compare BBQSORS as a transition source bridging LRDs and normal quasars with these objects. Their photometric data are shown in Figure 6 by solid lines with markers, overlaid with dashed lines indicating the SED fitting with blackbody components of different effective temperatures and modified by dust extinction. We also compare these candidates of the transitioning LRD with the stacked LRD photometry at $z = 6$ (Akins et al. 2025).

In the scenario where LRDs are AGNs whose SMBHs are enshrouded by dense gas envelopes, their stacked photometry can be reproduced by a blackbody component of $T_{\rm eff} = 4500$ K without visual extinction or of $T_{\rm eff} = 7000$ K

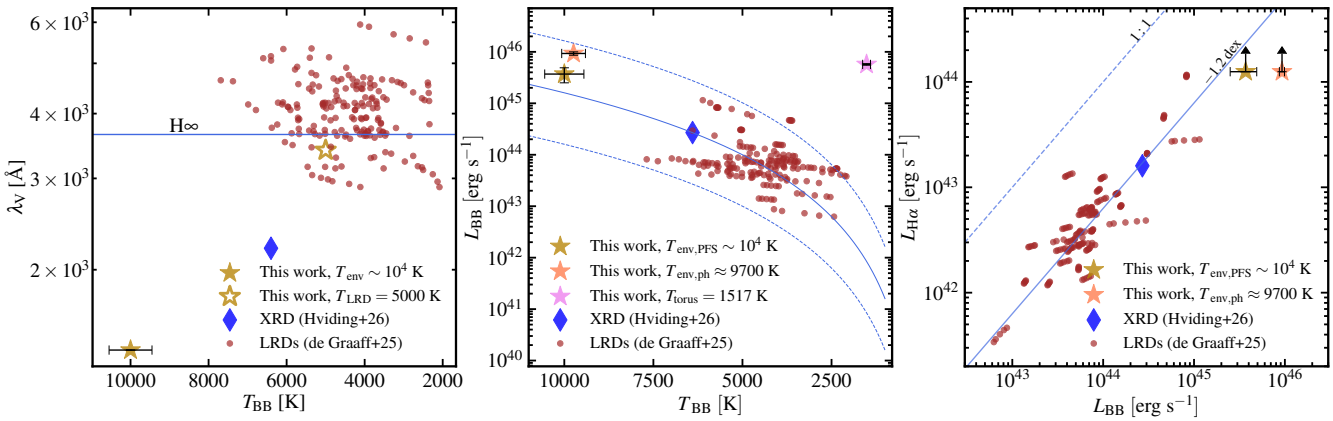

Figure 7. We compare the blackbody temperature $T_{\rm BB}$ and luminosity $L_{\rm BB}$, the rest-frame wavelength $\lambda_{\rm rest}$ at which the V-shaped feature emerges, and the Hα luminosity of BBQSORS with those of LRDs at $z < 4.5$ from de Graaff et al. (2025) and the XRD from Hviding et al. (2026). The solid line in $\lambda_{\rm V}$–$T_{\rm BB}$ indicates the Balmer limit. In the middle panel, we derive the $L_{\rm BB}$–$T_{\rm BB}$ relation (solid line) adopting a fiducial LRD-like photosphere radius (Inayoshi & Ho 2025) and shift it by ±1 dex (dashed lines). In the $L_{\rm H\alpha}$–$L_{\rm BB}$ plane, we show the 1 : 1 relation (dashed line) between the two and shift it by −1.2 dex (solid line).

and reddened by $A_{\rm V} = 2$ (Kido et al. 2025). The absence of an AGN dust torus, or that the dust torus has just started to form, leads to the overall non-detection of radiation from LRDs in the MIR regime. For XRD and Forge sources, their optical-–NIR continua can be modeled with a single blackbody component at temperatures of $T_{\rm eff} \sim$ (5–6) $\times 10^3$ K as well. In the MIR regime, the absence of dedicated MIR observations prevents a firm assessment of whether a dust torus is present in the XRD. Notably, however, the 1–6 μm photometry of Forge sources exhibits strong similarities to BBQSORS and can be well reproduced by a blackbody component with $T \sim 1200$ K, suggestive of the emergence of a dust torus (or alternatively $T \sim 500$ K; see Fu et al. 2025 for further discussion). Hence, the XRD and Forges populations are likely to represent an intermediate evolutionary phase as the LRDs transition toward BBQSORS, accompanied by the progressive development of a dust torus and the expansion of the photosphere.

We estimated the SMBH mass of BBQSORS using the broad Mg IIλ2800 emission line fitted by `S`^{3}`Fit`, which has been corrected for the strong Fe II emission. We adopted the empirical relation $M_{\rm BH} = 10^{6.79\pm0.55} \left[\frac{\rm FWHM(MgII)}{1000\ \rm km\ s^{-1}}\right]^2 \left(\frac{L_{2100\text{Å}}}{\rm erg\ s^{-1}}\right)^{0.5}$ (Vestergaard & Osmer 2009), where $L_{2100\text{Å}}$ is calculated from the PFS spectrum considering $A_{\rm V} = 0.09$, resulting in $M_{\rm BH} = 2.5^{+6.3}_{-1.8} \times 10^8\ M_\odot$. The luminosity of the dust torus is $(5.7 \pm 0.2) \times 10^{45}$ erg s^{-1}. For the envelope luminosity, we take the best-fit value of the PFS spectrum, which is $L_{\rm env,PFS} = (3.7 \pm 1.2) \times 10^{45}$ erg s^{-1}, as a conservative estimate. Treating the AGN bolometric luminosity as $L_{\rm AGN,bol} \sim L_{\rm env,PFS} + L_{\rm torus}$, the Eddington ratio of BBQSORS is $\lambda_{\rm Edd} \approx 0.28^{+1.00}_{-0.08}$. These properties are comparable to those of Forge sources, although it should noted that the mass estimate remains somewhat uncertain because the UV radiation of BBQSORS originates from the SMBH envelope rather than from a standard thin disk. On the other hand, the VLA-COSMOS deep 3 GHz radio observations of the two Forge sources have flux densities about $\approx$ 15 μJy and 84 μJy, corresponding to $L_{\rm 3GHz} \sim 1 \times 10^{24}$ W Hz^{-1} and $L_{\rm 3GHz} \sim 6 \times 10^{24}$ W Hz^{-1}, respectively, to be compared with $L_{\rm 3GHz} \sim 5 \times 10^{26}$ W Hz^{-1} of BBQSORS. Therefore, the potential merger event of BBQSORS may trigger the outburst of the radio jet (e.g. Zhong et al. 2024), facilitating the fragmentation of the SMBH envelope.

In Figure 7, we further compare the blackbody temperature $T_{\rm BB}$ and luminosity $L_{\rm BB}$ of the SMBH envelope, the rest-frame wavelength $\lambda_{\rm rest}$ of the V-shaped feature, and the Hα luminosity of BBQSORS with corresponding quantities for LRDs at $z < 4.5$ (de Graaff et al. 2025) and the XRD (Hviding et al. 2026). In the middle panel, we consider an LRD-like photosphere with a fiducial radius determined by $R_{\rm ph} = \sqrt{L_{\rm ph}/4\pi\sigma_{\rm SB}T_{\rm eff}^4}$ (Inayoshi & Ho 2025), where $\sigma_{\rm SB}$ is the Stefan-Boltzmann constant, assuming $L_{\rm ph} = 1 \times 10^{44}$ erg s^{-1}, and $T_{\rm eff} = 5000$ K. Fixing $R_{\rm ph}$ and assuming $L_{\rm ph} \simeq L_{\rm BB,LRD}$, we plot the solid line indicating how $L_{\rm ph}$ evolves with the effective temperature. The luminosity of Hα of BBQSORS was estimated from the spectrophotometry of the Spectro-Photometer for the History of the Universe, Epoch of Reionization, and Ices Explorer (SPHEREx) and fitted by `S`^{3}`Fit` (see Appendix A). Owing to the low spectral resolution and noisy flux measurements, the Hα line has a measured FWHM $\approx$ 2100±1800 km s^{-1}. This value is significantly lower than those of C III]λ1909 and Mg IIλ2800, potentially leading to an underestimate of $L_{\rm H\alpha}$. Overall, BBQSORS lies broadly consistent with the $L_{\rm BB}$–$T_{\rm BB}$ and $L_{\rm H\alpha}$–$L_{\rm BB}$ relations established for LRDs, supporting its identification as a strong candidate for an evolved LRD.

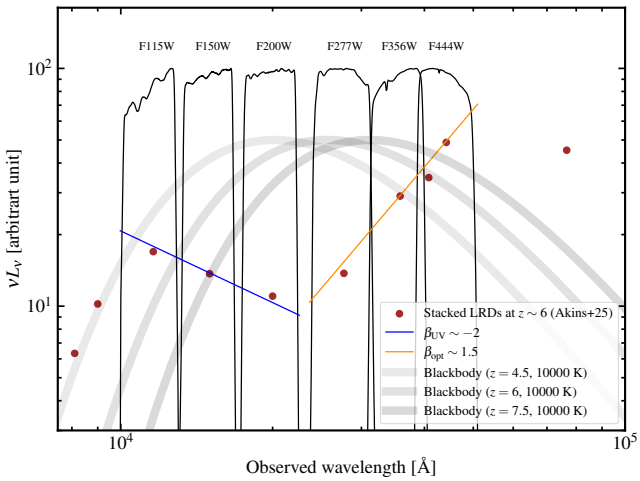

Figure 8. We plot the simple blackbody spectrum with $T = 10^4$ K at different redshifts, overlaid with stacked LRD photometry at $z = 6$ and JWST NIRCAM filters whose transmissions are normalized. High-z LRDs are selected according their V-shapes while transitioning LRDs characterized by blackbody quasars exhibit the Λ-shape.

3.3. *Why LRD color-color selections do not find $T \sim 10^4$K blackbody sources?*

Current LRD color–color selection criteria require four photometric bands sampling the V-shaped feature, two bands on the blue side and additional two bands on the red side, while excluding a band at the V-shaped minimum, in order to mitigate contamination from emission lines. In such a way, the current JWST cannot choose the appropriate $T \sim 10^4$ K sources because the bluest JWST/NIRCam band will cover "bluer" the Lyα break for those at $z \gtrsim 6$. This makes the color redder in the blue part and bluer in the red part. The same situation happens if using F115W to F444W to cover the blackbody spectrum, as shown in Figure 8. On the contrary of LRDs, this population of possible transitioning LRDs could exhibit a red UV continuum of $\beta_{\rm UV} \approx 1.5$ and a blue optical continuum of $\beta_{\rm opt} \approx -2$. Resultantly, sources bridging LRDs and normal quasars have been overlooked.

4. CONCLUSION

In this Letter, we report Subaru/PFS observation of a radio-loud quasar, BBQSORS, at $z_{\rm CIII} = 1.715$ and residing in a potential galaxy merger. The PFS UV spectrum covering $\sim$ 1500–3500 Å in the rest-frame displays three distinguished features. The first feature is the presence of broad C III]λ1909 and Mg IIλ2800 emission lines, with FWHM $\gtrsim$ 3400 km s^{-1}, accompanied by Al III$\lambda\lambda$1855, 1863 and Mg II$\lambda\lambda$2796, 2803 absorption doublets. The second feature is the strong Fe II continuum emission in the vicinity of Mg IIλ2800. The third feature is the significantly curved underlying continuum, exhibiting a Λ-shape. Globally, the spectrum can be well reproduced by a single blackbody spectrum with an effective temperature of 10000 K.

The UV–MIR photometric data of BBQSORS can be fitted by introducing three blackbody components: an SMBH envelope of $T \approx 9700$ K, an AGN dust torus of $T \approx 1500$ K, and galactic dust of $T \approx 80$ K. Notably, we found an excess in the flux density of GALEX NUV, which cannot be included in the blackbody model. By interpolating the GALEX NUV data assuming a power law continuum with $\beta_\lambda = -2$, the resulting power law spectrum, combining the blackbody spectrum, exhibits the characteristic V-shaped SED observed in LRDs. Furthermore, when the blackbody spectrum of BBQSORS is scaled to an effective temperature representative of LRDs, $T \approx 5000$ K, the UV power law intersects the blackbody component, producing a V-shaped feature around 3400 Å.

These results suggest that BBQSORS is likely to be transitioning from an LRD-like state to a normal quasar. At this evolutionary stage, the SMBH envelope begins to disperse, as accretion onto the SMBH is no longer sufficient to replenish the envelope mass, and as strong feedback from radiation and radio jets drives further mass loss. Future NIR observations are needed to search for the Hα absorption feature commonly observed in LRDs, as well as the Balmer break expected from an optically thick envelope. Measurements of the gas metallicity and direct evidence for outflows would provide further tests of whether BBQSORS represents an evolved LRD in a bloated-envelope phase.

ACKNOWLEDGMENTS

We thank Jong-Hak Woo for fruitful discussions. Y.Z. is supported by Japan Society for the Promotion of Science Research Fellowship for Young Scientists. This work is supported by the Japan Society for the Promotion of Science (JSPS) KAKENHI (25K01043; K. Ichikawa). K.I. also acknowledges support from the JST FOREST Program, Grant Number JPMJFR2466 and the Inamori Research Grants, which helped make this research possible.

Facilities: Subaru/PFS, Subaru/HSC, *GALEX*, *WISE*, *Spitzer*, *XMM-Newton*, *VLA*

APPENDIX

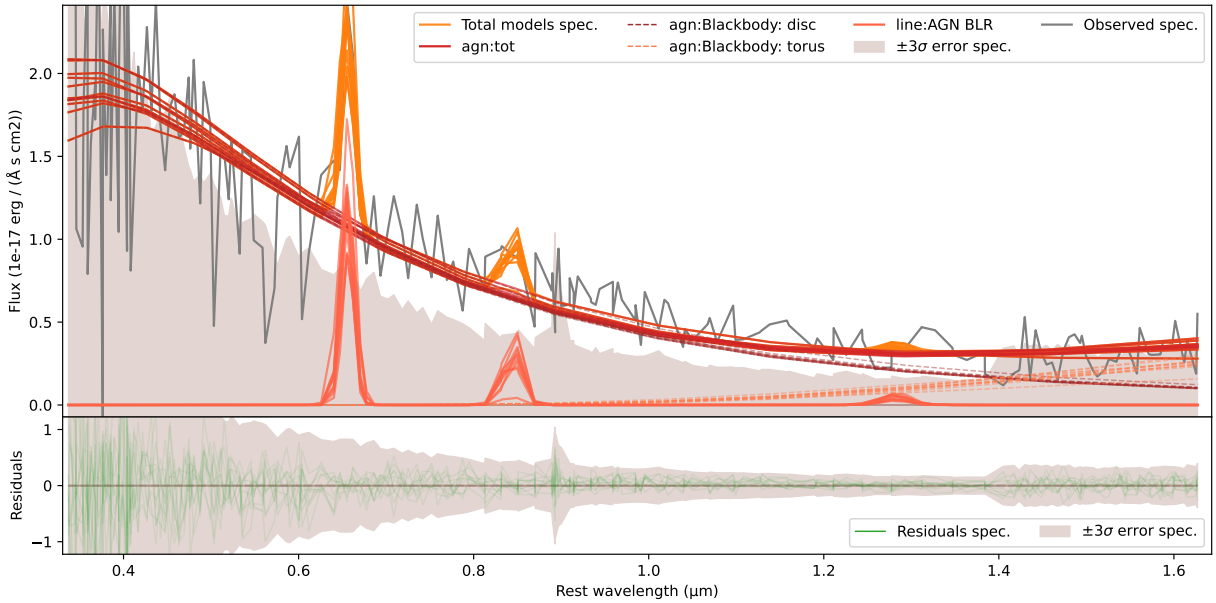

Figure 9. SPHEREx spectrophotometry (gray solid line) fitted by `S3Fit`. From left to right, peaks of the modeled line components indicate Hα, O Iλ8446, and Paβ.

A. SPHEREX SPECTROPHOTOMETRY

We show the SPHEREx spectrophotometry, covering 0.4–1.6 μm in the rest-frame, fitted by `S3Fit` in Figure 9. The underlying continua, as revealed in Figure 3, are assumed to be a composition of SMBH envelope and dust torus blackbody components. This spectrophotometry exhibits a robust detection of Hα, while detections of O Iλ8446 and Paβ are only marginal. Due to the low resolution, it is not feasible in this stage to determine whether there exist absorption features associated with Balmer series, and the FWHM of Hα cannot be reliably measured.

Current fits find FWHM(Hα) $\approx 2100 \pm 1800$ km s^{-1} and $F_{\rm H\alpha} = (5.98 \pm 1.53) \times 10^{15}$ erg/s/cm^2, resulting in $L_{\rm H\alpha} = (1.25 \pm 0.33) \times 10^{44}$ erg s^{-1} after correcting for the resolution. With these measurements, we estimated the SMBH mass following (Shen et al. 2011)

$$\log\left(\frac{M_{\rm BH,H\alpha}}{M_\odot}\right) = 0.379 + 0.43\log\left(\frac{L_{\rm H\alpha}}{10^{42}\ {\rm erg\ s^{-1}}}\right) + 2.1\log\left(\frac{\rm FWHM_{H\alpha}}{\rm km\ s^{-1}}\right). \quad \text{(A1)}$$

Resultantly, we find $M_{\rm BH,H\alpha} = 1.8^{+5.6}_{-1.8} \times 10^8\ M_\odot$, in loose agreement with $M_{\rm BH,MgII} = 2.5 \times 10^8\ M_\odot$. Nonetheless, these values should be handled with caution since we simply treat the observed Hα as the broad component originating from the BLR. High-resolution spectroscopy is mandatory to confirm these numbers.

REFERENCES

Ahumada, R., Allende Prieto, C., Almeida, A., et al. 2020, ApJS, 249, 3, doi: 10.3847/1538-4365/ab929e

Aihara, H., Arimoto, N., Armstrong, R., et al. 2018, PASJ, 70, S4, doi: 10.1093/pasj/psx066

Akins, H. B., Casey, C. M., Lambrides, E., et al. 2025, ApJ, 991, 37, doi: 10.3847/1538-4357/ade984

Ananna, T. T., Bogdán, Á., Kovács, O. E., Natarajan, P., & Hickox, R. C. 2024, ApJL, 969, L18, doi: 10.3847/2041-8213/ad5669

Begelman, M. C., & Dexter, J. 2026, ApJ, 996, 48, doi: 10.3847/1538-4357/ae274a

Chen, K., Li, Z., Inayoshi, K., & Ho, L. C. 2025a, ApJL, 994, L42, doi: 10.3847/2041-8213/ae1955

Chen, X. 2025, S3Fit: Simultaneous Spectrum and photometric-SED Fitting code for galaxy observations, Astrophysics Source Code Library, record ascl:2503.024

Chen, X., Ichikawa, K., Akiyama, M., et al. 2025b, arXiv e-prints, arXiv:2510.02801, doi: 10.48550/arXiv.2510.02801

Cova, F., Gastaldello, F., Wik, D. R., et al. 2019, A&A, 628, A83, doi: 10.1051/0004-6361/201834644

Cutri, R. M., Wright, E. L., Conrow, T., et al. 2021, VizieR Online Data Catalog: AllWISE Data Release (Cutri+ 2013), VizieR On-line Data Catalog: II/328. Originally published in: IPAC/Caltech (2013)

de Graaff, A., Hviding, R. E., Naidu, R. P., et al. 2025, arXiv e-prints, arXiv:2511.21820, doi: 10.48550/arXiv.2511.21820

Fawcett, V. A., Alexander, D. M., Rosario, D. J., et al. 2022, MNRAS, 513, 1254, doi: 10.1093/mnras/stac945

Fu, S., Zhang, Z., Jiang, D., et al. 2025, arXiv e-prints, arXiv:2512.02096, doi: 10.48550/arXiv.2512.02096

Gabriel, C., Denby, M., Fyfe, D. J., et al. 2004, Astronomical Society of the Pacific Conference Series, Vol. 314, The XMM-Newton SAS - Distributed Development and Maintenance of a Large Science Analysis System: A Critical Analysis, ed. F. Ochsenbein, M. G. Allen, & D. Egret, 759

Gwyn, S., McConnachie, A. W., Cuillandre, J.-C., et al. 2025, AJ, 170, 324, doi: 10.3847/1538-3881/ae03ab

Hall, P. B., Anderson, S. F., Strauss, M. A., et al. 2002, ApJS, 141, 267, doi: 10.1086/340546

Hopkins, P. F., Strauss, M. A., Hall, P. B., et al. 2004, AJ, 128, 1112, doi: 10.1086/423291

Hosokawa, T., Omukai, K., & Yorke, H. W. 2012, ApJ, 756, 93, doi: 10.1088/0004-637X/756/1/93

Hosokawa, T., Yorke, H. W., Inayoshi, K., Omukai, K., & Yoshida, N. 2013, ApJ, 778, 178, doi: 10.1088/0004-637X/778/2/178

Hviding, R. E., de Graaff, A., Liu, H., et al. 2026, arXiv e-prints, arXiv:2601.09778, doi: 10.48550/arXiv.2601.09778

Inayoshi, K. 2025, ApJL, 988, L22, doi: 10.3847/2041-8213/adea66

Inayoshi, K., & Ho, L. C. 2025, arXiv e-prints, arXiv:2512.03130, doi: 10.48550/arXiv.2512.03130

Inayoshi, K., Kimura, S. S., & Noda, H. 2025, PASJ, 77, 811, doi: 10.1093/pasj/psaf050

Inayoshi, K., & Maiolino, R. 2025, ApJL, 980, L27, doi: 10.3847/2041-8213/adaebd

Inayoshi, K., Visbal, E., & Haiman, Z. 2020, ARA&A, 58, 27, doi: 10.1146/annurev-astro-120419-014455

IRSA, & SSC. 2020, Spitzer Enhanced Imaging Products, NASA IPAC DataSet, IRSA433, doi: 10.26131/IRSA433

Ji, X., Maiolino, R., Übler, H., et al. 2025, MNRAS, 544, 3900, doi: 10.1093/mnras/staf1867

Juodžbalis, I., Ji, X., Maiolino, R., et al. 2024, MNRAS, 535, 853, doi: 10.1093/mnras/stae2367

Kido, D., Ioka, K., Hotokezaka, K., Inayoshi, K., & Irwin, C. M. 2025, MNRAS, 544, 3407, doi: 10.1093/mnras/staf1898

Klindt, L., Alexander, D. M., Rosario, D. J., Lusso, E., & Fotopoulou, S. 2019, MNRAS, 488, 3109, doi: 10.1093/mnras/stz1771

Kocevski, D. D., Onoue, M., Inayoshi, K., et al. 2023, ApJL, 954, L4, doi: 10.3847/2041-8213/ace5a0

Kocevski, D. D., Finkelstein, S. L., Barro, G., et al. 2025, ApJ, 986, 126, doi: 10.3847/1538-4357/adbc7d

Kokubo, M., & Harikane, Y. 2025, ApJ, 995, 24, doi: 10.3847/1538-4357/ae119e

Labbe, I., Greene, J. E., Matthee, J., et al. 2024, arXiv e-prints, arXiv:2412.04557, doi: 10.48550/arXiv.2412.04557

Lacy, M., Baum, S. A., Chandler, C. J., et al. 2020, PASP, 132, 035001, doi: 10.1088/1538-3873/ab63eb

Leccardi, A., & Molendi, S. 2008, A&A, 486, 359, doi: 10.1051/0004-6361:200809538

Li, Z., Inayoshi, K., Chen, K., Ichikawa, K., & Ho, L. C. 2025, ApJ, 980, 36, doi: 10.3847/1538-4357/ada5fb

Lin, X., Wang, F., Fan, X., et al. 2024, ApJ, 974, 147, doi: 10.3847/1538-4357/ad6565

Ma, Y., Greene, J. E., Setton, D. J., et al. 2025a, arXiv e-prints, arXiv:2504.08032, doi: 10.48550/arXiv.2504.08032

Ma, Y., Greene, J. E., Volonteri, M., et al. 2025b, arXiv e-prints, arXiv:2509.02662, doi: 10.48550/arXiv.2509.02662

Magnier, E. A., Schlafly, E. F., Finkbeiner, D. P., et al. 2020, ApJS, 251, 6, doi: 10.3847/1538-4365/abb82a

Matthee, J., Naidu, R. P., Brammer, G., et al. 2024, ApJ, 963, 129, doi: 10.3847/1538-4357/ad2345

Planck Collaboration, Aghanim, N., Akrami, Y., et al. 2020, A&A, 641, A6, doi: 10.1051/0004-6361/201833910

Richards, G. T., Hall, P. B., Vanden Berk, D. E., et al. 2003, AJ, 126, 1131, doi: 10.1086/377014

Richards, G. T., Lacy, M., Storrie-Lombardi, L. J., et al. 2006, ApJS, 166, 470, doi: 10.1086/506525

Rosario, D. J., Alexander, D. M., Moldon, J., et al. 2021, MNRAS, 505, 5283, doi: 10.1093/mnras/stab1653

Schneider, A. C., Vrba, F. J., Bruursema, J., et al. 2025, AJ, 170, 86, doi: 10.3847/1538-3881/ade43c

Setton, D. J., Greene, J. E., Spilker, J. S., et al. 2025, ApJL, 991, L10, doi: 10.3847/2041-8213/ade78b

Shen, Y., Richards, G. T., Strauss, M. A., et al. 2011, ApJS, 194, 45, doi: 10.1088/0067-0049/194/2/45

Tamura, N., Yabe, K., Koshida, S., et al. 2024, in Society of Photo-Optical Instrumentation Engineers (SPIE) Conference Series, Vol. 13096, Ground-based and Airborne Instrumentation for Astronomy X, ed. J. J. Bryant, K. Motohara, & J. R. D. Vernet, 1309605, doi: 10.1117/12.3015967

Tanaka, T. S., Akins, H. B., Harikane, Y., et al. 2025, ApJ, 995, 21, doi: 10.3847/1538-4357/ae145f

Taylor, A. J., Kokorev, V., Kocevski, D. D., et al. 2025, ApJL, 989, L7, doi: 10.3847/2041-8213/ade789

Trefoloni, B., Ji, X., Maiolino, R., et al. 2025, A&A, 700, A203, doi: 10.1051/0004-6361/202452795

Tsuzuki, Y., Kawara, K., Yoshii, Y., et al. 2006, ApJ, 650, 57, doi: 10.1086/506376

Urrutia, T., Becker, R. H., White, R. L., et al. 2009, ApJ, 698, 1095, doi: 10.1088/0004-637X/698/2/1095

Vanden Berk, D. E., Wesolowski, S. C., Yeckley, M. J., et al. 2020, MNRAS, 493, 2745, doi: 10.1093/mnras/staa411

Véron-Cetty, M.-P., Joly, M., & Véron, P. 2004, A&A, 417, 515, doi: 10.1051/0004-6361:20035714

Vestergaard, M., & Osmer, P. S. 2009, ApJ, 699, 800, doi: 10.1088/0004-637X/699/1/800

Vestergaard, M., & Wilkes, B. J. 2001, ApJS, 134, 1, doi: 10.1086/320357

Wang, T., Ferland, G. J., Yang, C., Wang, H., & Zhang, S. 2016, ApJ, 824, 106, doi: 10.3847/0004-637X/824/2/106

Webb, N. A., Coriat, M., Traulsen, I., et al. 2020, A&A, 641, A136, doi: 10.1051/0004-6361/201937353

Williams, C. C., Alberts, S., Ji, Z., et al. 2024, ApJ, 968, 34, doi: 10.3847/1538-4357/ad3f17

Willingale, R., Starling, R. L. C., Beardmore, A. P., Tanvir, N. R., & O'Brien, P. T. 2013, MNRAS, 431, 394, doi: 10.1093/mnras/stt175

Yue, M., Eilers, A.-C., Ananna, T. T., et al. 2024, ApJL, 974, L26, doi: 10.3847/2041-8213/ad7eba

Zhang, Z., Jiang, L., Liu, W., & Ho, L. C. 2025a, ApJ, 985, 119, doi: 10.3847/1538-4357/adcb3e

Zhang, Z., Li, M., Oguri, M., et al. 2025b, arXiv e-prints, arXiv:2512.05180, doi: 10.48550/arXiv.2512.05180

Zhong, Y., Inoue, A. K., Sugahara, Y., et al. 2024, MNRAS, 529, 4531, doi: 10.1093/mnras/stae798

Zhong, Y., Ichikawa, K., Hildebrandt, H., et al. 2025, ApJS, 281, 22, doi: 10.3847/1538-4365/ae03c3